Published in final edited form as:
Dev Cell. 2010 May 18; 18(5): 713–724. doi:10.1016/j.devcel.2010.02.016.

VEGF receptor 2 endocytic trafficking regulates arterial morphogenesis

Anthony A. Lanahan[1], **Karlien Hermans**[2], **Filip Claes**[2], **Joanna S. Kerley-Hamilton**[3], **Zhen W. Zhuang**[1], **Frank J. Giordano**[1], **Peter Carmeliet**[2], and **Michael Simons**[1,4]

[1]Section of Cardiovascular Medicine, Department of Internal Medicine, Yale University School of Medicine, New Haven, CT 06520

[2]Vesalius Research Center, VIB-Vlaams Instituut voor Biotechnologie, 3000 Leuven, Belgium

[3]Section of Cardiology, Department of Medicine, Dartmouth Medical School, Lebanon, NH 03756

[4]Department of Cell Biology, Yale University School of Medicine, New Haven, CT 06520

Abstract

VEGF is the key growth factor regulating arterial morphogenesis. However, molecular events involved in this process have not been elucidated. Synectin null mice demonstrate impaired VEGF signaling and a marked reduction in arterial morphogenesis. Here we show that this occurs due to delayed trafficking of VEGFR2-containing endosomes that exposes internalized VEGFR2 to selective dephosphorylation by PTP1b on Y^{1175} site. Synectin involvement in VEGFR2 intracellular trafficking requires myosin-VI, and myosin-VI knockout in mice or knockdown in zebrafish phenocopy the synectin null phenotype. Silencing of PTP1b restores VEGFR2 activation and significantly recovers arterial morphogenesis in myosin-$VI^{-/-}$ knockdown zebrafish and synectin$^{-/-}$ mice. We conclude that activation of the VEGF-mediated arterial morphogenesis cascade requires phosphorylation of the VEGFR2 Y^{1175} site that is dependent on trafficking of internalized VEGFR2 away from the plasma membrane via a synectin-myosin-VI complex. This key event in VEGF signaling occurs at an intracellular site and is regulated by a novel endosomal trafficking-dependent process.

INTRODUCTION

VEGF plays a key role in arterial morphogenesis both during development and in the adult organism. While three receptors- VEGF-R1 (Flt-1), VEGFR2 (Flk-1) and neuropilin-1 bind VEGF-A, VEGFR2 signaling is considered crucial to vascular formation. In particular, phosphorylation of Y^{1175} in the VEGFR2 cytoplasmic domain is a key event as replacement of the VEGFR2 gene with a VEGFR2 construct carrying a single Y1175F mutation results in failure of vasculogenesis and embryonic lethality (Sakurai et al., 2005). The sequence of events involved in VEGF-dependent VEGFR2 activation and subsequent signaling is thus thought to include the conventional steps of a growth factor binding to its tyrosine kinase receptor on the

Address correspondence to: Prof. Michael Simons Section of Cardiovascular Medicine P.O. Box 208017 333 Cedar ST New Haven, CT 06520-8017 Phone: 203 785-7000 michael.simons@yale.edu.

plasma cell membrane followed by receptor dimerization, activation and assembly of a membrane-proximal signaling complex.

Previously we have described that deletion of synectin (*gipc1*), a single PDZ-domain scaffold protein, results in decreased arterial morphogenesis and branching and that synectin$^{-/-}$ endothelial cells demonstrate reduced sensitivity to VEGF stimulation (Chittenden et al., 2006). Synectin is a widely expressed protein isolated simultaneously by various laboratories as a binding partner of RGS-GAIP(De Vries et al., 1998), neuropilin-1 (Cai and Reed, 1999), semaphorin-4C (Wang et al., 1999), and syndecan-4 (Gao et al., 2000) among others. Its function remains unclear but it can control cell migration (Gao et al., 2000; Tkachenko et al., 2006), intracellular trafficking (Dance et al., 2004) and cell adhesion (Lanahan et al., 2006). Intracellular trafficking and endocytosis appear to be particularly important aspects of synectin function as suggested by recent studies (Valdembri et al., 2009; Varsano et al., 2006)

Of particular interest is synectin binding to myosin-VI, a retrograde motor involved in endosome transport (Naccache et al., 2006), suggesting the possibility that the synectin-myosin-VI dependent regulation of trafficking of a newly internalized receptor could potentially regulate its signaling. While the possibility of an intracellular site of signaling for VEGFR2 has been suggested (Lampugnani et al., 2006), the molecular events controlling VEGFR2 signaling from an endosome remain unknown.

Since arterial morphogenesis has been linked to VEGF, we examined in detail various events following VEGF stimulation of synectin$^{-/-}$ endothelial cells. We find that while VEGFR2 binding of VEGF-A_{165} and subsequent cellular uptake of the VEGF-VEGFR2 complex proceeds normally, VEGFR2 fails to enter the early endosomal compartment, remaining in close proximity to the plasma cell membrane. The trafficking of internalized VEGFR2 from the plasma membrane requires formation of the synectin-myosin-VI complex, and disruption of myosin-VI expression phenocopies synectin deletion. Abnormal VEGFR2 trafficking leads to decreased phosphorylation of the crucial Y^{1775} site and reduced activation of downstream signaling via PLCγ/MAPK and PI3-Kinase/Akt pathways. This, in turn, occurs due to activity of a small intracellular tyrosine phosphatase PTP1b as suppression of PTP1b expression restores VEGF signaling in this system.

Thus, synectin-myosin-VI-dependent trafficking of VEGFR2 plays a key role in the regulation of arterial morphogenesis by moving the VEGFR2 containing endosomes away from PTP1b-rich peri-plasma cell membrane environment.

RESULTS

Impaired VEGFR2 activation in response to VEGF stimulation in synectin$^{-/-}$ arterial endothelial cells

We have previously demonstrated that synectin$^{-/-}$ arterial endothelial cells (AEC) have reduced responsiveness to VEGF stimulation (Chittenden et al., 2006; Prahst et al., 2008). To further detail this observation and to establish the underlying cause, we examined VEGF signaling responses and VEGFR2 activation in synectin$^{-/-}$ and wild type AEC.

VEGF stimulation of synectin$^{-/-}$ AEC resulted in decreased activation of key downstream signaling effects including activation of Akt and p42/44 MAPK (ERK-1/2) (Fig 1A,B). To explore the reason for this finding, we first examined total and cell surface expression of VEGF receptors R1 and R2 in AEC derived from synectin$^{-/-}$ and littermate synectin$^{+/+}$ mice. No significant differences in receptor expression were noted by Western blotting of total cell lysates (Fig 1E, F) or cell-surface biotinylated proteins (Fig 1C, D).

Since VEGFR2 phosphorylation on key tyrosine residues is necessary for activation of VEGF signaling, we next examined the status of Y^{1054} (a marker of general VEGFR2 activation) and Y^{1175} (PLCγ/MAPK and PI3K activation site). There were no significant changes in Y^{1054} phosphorylation suggesting that VEGFR2 was dimerizing and phosphorylating itself (Fig 1E). However, there was a pronounced reduction in Y^{1175} phosphorylation, corresponding to observed decreases in p42/44 MAPK and Akt activation (Fig 1F,G).

To further confirm these changes in VEGFR2 phosphorylation, we have examined additional downstream signaling events. In particular, reduced phosphorylation of Y^{1175} can be expected to result in decreased activation of PLCγ thereby leading to a decrease in the rise of intracellular calcium. Indeed, Western blotting demonstrated reduced PLCγ phosphorylation (Fig 1H and Fig S1A and Supplementary information) and reduced VEGF-induced Ca^{2+} flux (Fig 1I).

Myosin-VI is a synectin binding partner involved in regulation of VEGFR2 activation

We next sought to identify synectin binding partners responsible for regulation of VEGFR2 activity. Since synectin binds neuropilin and neuropilin signaling is impaired in synectin null endothelial cells (Prahst et al., 2008), it is possible that the lack of this interaction is responsible for decreased VEGFR2 activation in synectin$^{-/-}$ AEC. To evaluate this possibility, we examined ERK1/2 activation following treatment with VEGF-D, a VEGF family member that signals via VEGFR2 in a neuropilin-independent manner. Similar to VEGF-A, VEGF-D treatment resulted in reduced activation of p42/44 MAPK and Akt in synectin$^{-/-}$ AEC (Fig S1B) suggesting that defective VEGFR2 signaling in synectin$^{-/-}$ AEC is not explained by the lack of a neuropilin-1-synectin interaction.

Synectin can bind other cytoplasmic proteins via its PDZ domain and it also binds myosin-VI. To further evaluate potential contributions of synectin binding proteins to impaired VEGF signaling, synectin$^{-/-}$ AEC were transduced with an adenoviral construct carrying either a full-length wild type synectin cDNA (Ad-Syn), a synectin construct with a mutated PDZ domain (Ad-Syn-PDZ^{-}) or deleted myosin-VI-binding domain (Ad-Syn-MVI^{-}). Transduction of synectin$^{-/-}$ AEC with Ad-Syn virus fully restored Y^{1175} site phosphorylation and Erk-1/2 activation by VEGF (Fig 2A). On the other hand, transduction with either Ad-Syn-PDZ^{-} (Fig 2B) or Ad-Syn-MVI^{-} (Fig 2C) constructs did not restore Erk-1/2 activation or Y^{1175} phosphorylation.

To confirm that myosin-VI is indeed involved in regulation of VEGF signaling, we examined VEGF-dependent endothelial cell responses in myosin-VI$^{-/-}$ AEC. Following treatment with VEGF-A, we observed decreased Erk-1/2 activation (Fig 2D, E) and reduced phosphorylation of VEGFR2 Y^{1175} site (Fig 2D, F) in myosin-VI$^{-/-}$ compared to myosin-VI$^{+/+}$ AEC.

Myosin-VI- synectin complex regulates VEGFR2 endocytosis

We then addressed the mechanism of myosin-VI-dependent regulation of VEGF signaling. Since both synectin and myosin VI are involved in intracellular transport of endocytic vesicles, we examined whether alterations in VEGFR2 endocytic trafficking may be responsible for the observed VEGF signaling abnormalities in synectin$^{-/-}$ and myosin-VI$^{-/-}$ AEC.

Cell surface VEGFR2 on synectin$^{-/-}$, myosin-VI$^{-/-}$ and control AEC were labeled with biotin and the cells were then exposed to VEGF-A_{165}. At fixed time intervals cell lysates were prepared and the amount of internalized VEGFR2 was determined by Western blotting (Fig 3A). There were no significant differences in VEGFR2 internalization between synectin and myosin-VI null AEC and normal AEC suggesting that neither protein was involved in the receptor internalization. FACS analysis of VEGFR2 uptake from the cell surface after VEGF

stimulation in synectin$^{-/-}$ and $^{+/+}$ AEC confirmed these observations (Fig S2 and Supplementary information).

We next examined the transport of VEGFR2-containing endosomes using wide field microscopy. Five minutes following VEGF stimulation of wild type AEC, VEGFR2 was readily detectable in association with the earliest population of endosomes defined by the presence of EEA1 and by 15 min over 50% of endocytosed receptors were detected in that endosomal compartment (Fig 3B,C). Remarkably, there was a pronounced delay in association of VEGFR2 with EEA1-postive endosomes in both synectin$^{-/-}$ (Fig 3B,C) and myosin-VI$^{-/-}$ (Fig 3B,D) AEC suggesting that the absence of either synectin or myosin VI interfered with trafficking of very early endosomes containing VEGFR2.

To examine the reason for this delayed association of VEGFR2-containing endosomes with EEA1 endosomes, we evaluated the motility of VEGFR2 vesicles using live cell imaging. After VEGF treatment the speed of movement and the mean step increment of VEGFR2-containing endosomes were significantly decreased in synectin$^{-/-}$ AEC (Fig 3E) and myosin-VI$^{-/-}$ AEC (not shown) in agreement with the decrease previously observed in myosin-VI null cells (Aschenbrenner et al., 2004)

To further explore how VEGFR2 endocytic trafficking affects its signaling, we knocked down two Rab GTPases responsible for either late endosomal recycling to the plasma membrane (Rab11) or for movement of endosomes to the lysosomes (Rab7) in AEC. In both cases there was a significant increase in VEGF-induced P-ERK activation (Fig 4D) consistent with the hypothesis that the VEGFR2 containing complex remained in the cytoplasm for an extended period of time. At the same time, we also observed decreased association of VEGFR2 endosomes with the Rab7 or Rab 11 -positive compartment (Fig 4A–C) in synectin$^{-/-}$ AEC.

Myosin-VI knockdown impairs arterial morphogenesis in zebrafish and mice

To demonstrate that the synectin / myosin-VI axis plays a key role in VEGF signaling, we evaluated the effect of reduced myosin-VI expression in zebrafish and mice and compared them to the previously described synectin phenotype. Two co-orthologues of mammalian myosin VI have been identified in zebrafish and their expression pattern has been previously described (Kappler et al., 2004; Seiler et al., 2004). Myosin VIb (*myo6b*) is expressed exclusively in hair cells of the inner ear and lateral line organ, while myosin VIa (*myo6a*) is more widely distributed throughout the head and trunk of zebrafish embryos from 1 to 5 days post fertilization (dpf). A whole-mount *in situ* hybridization using a zebrafish *myo6a* antisense or sense riboprobe at 28 hours post fertilization (hpf) analysis confirmed the previously reported ubiquitous expression of myo6a in neural tube and somites (Fig. 5A,B). Moreover, the dorsal aorta and posterior cardinal vein expressed myo6a (Fig. 5A,B), similar to the expression of synectin in zebrafish embryos (Chittenden et al., 2006).

Myo6a knockdown phenocopies synectin knockdown in arterial development

We then examined whether myo6a knockdown phenocopies the arterial defects observed after synectin knockdown. To that end, we injected in one-cell stage embryos the *myo6a*-specific antisense morpholino oligonucleotide Myo6a-ATG1 that selectively targets the *myo6a* translation initiation site (Supplementary information). Using an established luciferase fusion reporter assay, Myo6a-ATG1 dose-dependently suppressed translation of the reporter, indicating that it was effective, whereas the inverted control morpholino Myo6a-Ctr was ineffective, even at the highest dose tested (Fig S3A). Macroscopic inspection revealed that Myo6a-ATG1 dose-dependently affected the morphological integrity of the injected embryos. Upon injection of a maximal dose (10.5 ng per embryo), 36% of *myo6a* knockdown (myo6a^{KD}) embryos developed deformities or died during the first two dpf; these embryos

were excluded. The remainder of myo6a^{KD} embryos had a normal to slightly curved or shortened body shape; blood flow in their axial and intersomitic vessels was sluggish or absent by two dpf. Thereafter, most myo6a^{KD} embryos started to develop pericardial edema.

To visualize the vascular defects in myo6a^{KD} embryos in more detail, we knocked down myo6a in *Tg(Fli1:EGFP)^{y1}* zebrafish. In Myo6a-Ctr and buffer injected control embryos, blood vessels developed normally (Fig. 5C,E,G). At 16 hpf, angioblasts in control embryos migrated from the lateral plate mesoderm to the midline in an ordered zipper-like pattern, proceeding in an antero-posterior direction (Fig. 5C, Table S1). These endothelial progenitors assembled in a primitive vascular cord, which then developed into a luminizied dorsal aorta and posterior cardinal vein by 24 hpf. In 32% of myo6a^{KD} embryos, a fraction of angioblasts stalled along their path towards the midline at 16 hpf, while others appeared to migrate chaotically in a disorganized zipper-like pattern (Fig. 5D, Table S1). This abnormal migration of endothelial progenitors impaired dorsal aorta morphogenesis. Up to 77% of myo6a^{KD} embryos developed an abnormally thin aorta with a substantially reduced lumen size, appearing as a cord-like structure, while the posterior cardinal vein developed normally at 30 hpf (Table S1). Whole-mount immunostaining for GFP revealed a patent posterior cardinal vein in control and myo6a^{KD} embryos (Fig. 5E,F), while the aortic lumen was abnormally small in myo6a^{KD} embryos (Fig. 5E,F). Overall, the aberrant angioblast migration and impaired formation of the axial artery in myo6a^{KD} embryos closely resembled the early vessel defects in synectin^{KD} embryos (Chittenden et al., 2006).

When analyzing subsequent stages of vessel development, we observed that, in control embryos, primary (arterial) ISVs branched off from the aorta at 20 hpf and navigated dorsally up to the dorsolateral roof of the neural tube, where they split into a caudal and rostral branch, elongated and fused with branches of other segments to form the dorsal longitudinal anastamotic vessels (DLAV) by 48 hpf (Fig. 5G, Table S1). In myo6a^{KD} embryos, initial ISV sprouting was normal and occurred at the proper designated aortic sites. In synectin^{KD} embryos, a fraction of ISVs failed to branch off from the aorta (Chittenden et al., 2006). By contrast, all ISVs branched off normally from the aorta in myo6a^{KD} embryos, but in 48% of morphants, at least five of all ISVs stalled along their dorsal trajectory and failed to reach the roof of the neural tube, thereby partially impairing DLAV formation (Fig. 5H, Table S1). Also, endothelial cells of ISVs often appeared abnormally slender (Fig. 5 H). Thus, the ISV defects in myo6a^{KD} embryos are qualitatively similar, though quantitatively less severe than those induced by synectin knockdown. Altogether, the impaired formation of the dorsal aorta and its arterial ISV sprouts in myo6a^{KD} zebrafish embryos nearly phenocopied the arterial defects upon synectin knockdown. All blood vessel defects described were induced by Myo6a-ATG1 in a dose-dependent manner (Table S1). Moreover, this vascular phenotype was specific, since another non-overlapping morpholino targeting the translational start site of *myo6a*, Myo6a-ATG2, which dose-dependently suppressed translation of the luciferase fusion reporter (Fig. S3) caused indistinguishable vascular defects (Table S1).

Myo6a^{KD} causes similar arterial cell defects as synectin^{KD} in zebrafish

We previously demonstrated that synectin knockdown reduces the proliferation of arterial endothelial cells (Chittenden et al., 2006). To assess whether knockdown of myo6a caused comparable defects, we measured arterial proliferation in myo6a^{KD} embryos, using similar techniques as used for synectin knockdown. *Tg(Fli1:EGFP)^{y1}* embryos were incubated with BrdU at 20 hpf, allowed to grow until 30 hpf after which arterial and venous GFP^{+}BrdU^{+} endothelial cells were counted (Fig S4). While the number of proliferating venous endothelial cells was unaffected (1.63 ± 0.12 cells/section in myo6a^{KD} embryos versus 1.61 ± 0.14 cells/section in control embryos; N=9; P=0.83), endothelial proliferation was reduced in the aorta and ISVs of myo6a^{KD} embryos (1.41 ± 0.16 cells/section in myo6a^{KD} embryos versus 1.95 ±

0.18 cells/section in controls; N=9; P<0.05). These results suggest that knockdown of myo6a – albeit somewhat less than knockdown of synectin- impairs migration and proliferation of arterial but not venous endothelial cells.

Myosin-VI knockout impairs arterial morphogenesis in mice

Unlike zebrafish, only one myosin-VI gene is present in mice. Myosin-VI null mice, similar to synectin null mice, were smaller than their littermate wild type counterparts (17.9±2.9g vs. 22.5±3.9g, p<0.01). Micro-CT evaluation of vascular density demonstrated a smaller number of arteries in the renal (Fig 5I,J) and peripheral circulations (Fig 5K), similar to findings in synectin knockout mice.

To evaluate the effect of myosin-VI deletion on arterial morphogenesis in adult tissues, the common femoral artery of myosin-VI$^{-/-}$ and control littermate mice was ligated and the flow recovery was measured over time using laser-Doppler as previously described. Similar to synectin$^{-/-}$ mice, myosin-VI$^{-/-}$ mice demonstrated impaired recovery of lower limb blood flow consistent with impaired arterial growth (Fig 5L).

VEGFR2 dephosphorylation in synectin$^{-/-}$ and myosin-VI$^{-/-}$ endothelial cells

The delayed trafficking of VEGFR2 endosomes away from the plasma membrane and the observed increase in dephosphorylation of VEGFR2 in both synectin$^{-/-}$ and myosin-VI$^{-/-}$ endothelial cells may be due to prolonged exposure of activated VEGFR2 to membrane-resident or peri-membrane tyrosine phosphatases in these cells. To test this possibility and to identify the phosphatase involved we used siRNA to knockdown four different phosphotyrosine phosphatases in synectin$^{-/-}$ AEC (Fig S5A) while measuring ERK1/2 activation in response to VEGF. Knockdown of PTP1b was the most effective in restoring ERK activation in synectin$^{-/-}$ AEC (Fig 6A, B). Furthermore, there was a marked restoration of VEGFR2 phosphorylation at Y^{1175} (Fig 6A). However, knockdown of these phosphatases in control (wild type) AEC had no additional effect on ERK1/2 phosphorylation (Fig S5B). Of interest, PTP1b was expressed equally in arterial and venous endothelial cells and synectin deletion had no effect on its expression (Fig S5C)

To confirm the physiologic significance of restoration of VEGFR2 Y^{1175} phosphorylation, wild type and synectin$^{-/-}$ AEC were exposed to either PTP1b or control siRNA and the migration response to VEGF was measured. While synectin$^{-/-}$ AEC treated with control siRNA migrated significantly less than control AEC, exposure to PTP1b siRNA significantly increased migration, restoring it to control cell levels, consistent with the observed VEGFR2 Y^{1175} site activation (Fig 6C).

Knockdown of ptp1B rescues the arterial phenotype upon myo6a knockdown

In line with our *in vitro* findings, we anticipated that the arterial defects upon myo6a knockdown were the consequence of a prolonged exposure of VEGFR2 to the phosphatase activity of PTP1b thereby inhibiting downstream VEGF signaling. We therefore silenced ptp1b in *Tg(Fli1:EGFP)^{y1}* zebrafish embryos by using a ptp1b-specific morpholino, Ptp1b-ATG, which targets the ptp1b translation initiation site. Similar to the myo6a targeting morpholinos, Ptp1b-ATG dose-dependently blocked translation of the reporter in a chimeric luciferase reporter assay (Fig. S3B).

Consistent with previous reports (van der Sar et al., 1999), a dose of 6 ng Ptp1b-ATG did not induce gross morphological deformities or vessel defects (thin dorsal aorta, arrested ISV formation), neither did it impair circulation by 2 dpf (not shown; N=147). However, in co-injection experiments, Ptp1B-ATG partially rescued the characteristic vascular defects, induced by a maximal dose of Myo6a-ATG1 (not shown). In embryos, injected with 10.5 ng

Myo6A-ATG1, 71% and 62% of the embryos exhibited a thin aorta or arrested ISVs, respectively (N=90). By contrast, in embryos co-injected with 10.5 ng Myo6A-ATG1 and 6 ng Ptp1b-ATG, only 50% and 31% of embryos exhibited corresponding vascular defects (Fig 6D, N=179; P<0.05 and P<0.001, respectively by Chi-square analysis). Qualitatively similar results were obtained when a lower dose of 3 ng Ptp1b-ATG was co-injected with 10.5 ng Myo6A-ATG1 (not shown). Co-silencing of ptp1b and myo6a also prolonged embryonic survival; of 186 myo6a^{KD} embryos, 51.6% were severely malformed or deceased by 2 dpf; corresponding values were 42.4% for ptp1b^{KD}:myo6a^{KD} embryos (3 ng Ptp1b-ATG; N=203; P<0.05) and 24.5% for ptp1b^{KD}:myo6a^{KD} embryos (6 ng Ptp1b-ATG; N=237; P<0.001). Partial rescue of the dorsal aorta and ISV defects by *myo6a* knockdown was also achieved by co-injection of another *ptp1b*-specific morpholino, Ptp1b-Splice (N=144; P<0.05 for both vascular phenotypes). This Ptp1b-Splice morpholino targets the splice site between the first exon and intron of ptp1b and efficiently blocks splicing as evidenced by PCR amplification of the ptp1b region spanning the first intron boundary (Fig. S3C). In contrast, similar doses of the control morpholino Ptp1b-Ctr failed to rescue the myo6a knockdown phenotype: of ptp1b^{Crl}:myo6a^{KD} embryos, 72.7% and 62.8% suffered dorsal aorta and ISV defects, respectively (N=161).

Knockdown of ptp1B rescues the arterial phenotype in synectin null mice

We next tested the effectiveness of PTP1b suppression on restoration of VEGFR2 signaling and arterial morphogenesis in synectin$^{-/-}$ mice. To this end, synectin$^{-/-}$ and control mice were subjected to common femoral artery ligation while a PTP1b inhibitor was administered daily by oral gavage. Assessment of distal limb blood flow using laser-Doppler imaging demonstrated markedly accelerated recovery in the inhibitor treated synectin$^{-/-}$ mice with flow recovering to levels seen in control mice (Fig 7A). Control animals treated with the inhibitor demonstrated a tendency towards higher flows than untreated controls, however only reaching statistical significance on day 7. To evaluate the extent of arteriogenesis, micro-CT images of the limb circulation were obtained (Fig 7C). There was a highly statistically significant increase in small (>168μm) arteries in the inhibitor treated synectin$^{-/-}$ mice (Fig 7B) with most of the new arteries appearing in the non-ischemic thigh area (Fig 7C).

DISCUSSION

Recent studies have demonstrated that tyrosine kinase receptors in general and VEGFR2 specifically, signal not only from the plasma cell membrane but from endosomal compartments (Di Fiore and De Camilli, 2001; von Zastrow and Sorkin, 2007) and that disruption of endocytosis may affect receptor signaling (Lampugnani et al., 2006). However, specific molecular mechanisms involved in this endocytosis-dependent regulation of receptor signaling have not been established. Here we report that trafficking of VEGFR2 from the plasma membrane to EEA1-positive endosomes requires synectin-myosin-VI-dependent retrograde transport through the cortical zone and that any defects in this transport results in PTP1b-dependent dephosphorylation of the Y^{1175} site. This, in turn, leads to defective arterial morphogenesis both during embryonic development and in adult tissues.

VEGFR2 signaling is enabled by phosphorylation of several critical cytoplasmic domain tyrosine residues following VEGF-induced dimerization while a number of phosphotyrosine phosphatases are thought to be capable of extinguishing it. To date, PTP1b (Nakamura et al., 2008), TC-PTP (Mattila et al., 2008), VE-PTP (Mellberg et al., 2009; Nottebaum et al., 2008), Dep-1/CD148 (Lampugnani et al., 2003) and Shp2 have all been reported to variously regulate VEGFR2 signaling (Mitola et al., 2006).

In particular, PTP1b has been reported to specifically dephosphorylate the Y^{1175} site thereby affecting activation of the PLCγ-MAPK pathway (Nakamura et al., 2008). PTP1b is a small

cytoplasmic PTP (Bourdeau et al., 2005) that resides on the cytoplasmic surface of the endoplasmic reticulum. This is in direct distinction to another small cytoplasmic PTP, TC-PTP, that dephosphorylates VEGFR2 at $Y^{1054/1059}$ (TK activation site) and Y^{1214} (p38MAPK activation site) sites while not affecting Y^{1175}.

PTP1b expression is controlled by a number of factors such as ischemia and hypoxia, and increased expression is noted in insulin-resistant states and obesity (Bourdeau et al., 2005), conditions associated with decreased VEGF activity. PTP1b-catalyzed dephosphorylation requires endocytosis of the receptors and occurs at specific sites on the surface of the endoplasmic reticulum (Haj et al., 2002). PTP1b co-precipitates with VEGFR2 (Nakamura et al., 2008), suggesting either a physical interaction between the two proteins or their presence in the same protein complex. A decrease in PTP1b expression results in increased ERK1/2 activation, while an increase in its expression suppresses it (Nakamura et al., 2008). This suggests that PTP1b activity specifically affects the Y^{1175} site phosphorylation that is required for binding of PLCγ and subsequent activation of the RAF-MEK-ERK cascade.

PTP1b effects are not restricted to VEGFR2. Of interest to the current study is the observation that PTP1b inhibits EGF-R signaling from the endocytic compartment (Eden et al., 2009) by regulating phosphorylation of the PLCγ binding site (Y^{992}) in EGFR (Milarski et al., 1993).

Transmembrane receptor type PTPs also have been reported to regulate VEGFR2 activity. Thus, DEP1/CD148 by binding to β-catenin and p120-catenin associates with VE-cadherin-VEGFR2 complex on the plasma cell membrane and dephosphorylates VEGFR2 (Lampugnani et al., 2006). A depletion of DEP1 leads to increased tyrosine phosphorylation of all major VEGFR2 autophosphorylation sites but surprisingly results only in activation of Src activity without an overall stimulation of VEGF-dependent signaling (Chabot et al., 2009). VE-PTP, a transmembrane PTP structurally related to DEP-1, is expressed in the vasculature during development with a preferential expression in arterial endothelium. A reduction in VEGFR2-VEPTP association leads to a striking increase in receptor phosphorylation at most sites with the possible exception of Y^{1214} (Mellberg et al., 2009).

Thus, while various PTPs are able to affect VEGFR2 signaling, their sites of action are distinct and specific for the each enzyme. Since VEGFR2 endocytosis is thought to play a major role in regulation of its signaling, it is important to link the two events in terms of molecular mechanism. VEGFR2 internalizes predominantly in a clathrin-dependent manner in EEA1-positive endosomes and to a very low extent via caveolin or lipid raft pathways. Furthermore, active PLCγ co-distributes with internalized VEGFR2, suggesting that Y^{1175} site phosphorylation either occurs in or is maintained in endosomes. Reduction in clathrin expression results in decreased VEGFR2 and ERK1/2 phosphorylation (Lampugnani et al., 2006).

While little is known about the transport of newly endocytosed proteins in clathrin-coated vesicles to early endosomes, recent studies have implicated synectin as an important regulator of this step. Thus, synectin is involved in endocytosis of TrkA (Lin et al., 2006; Lou et al., 2001; Varsano et al., 2006), Glut1 (Wieman et al., 2009), and neuropilin-1 (Valdembri et al., 2009). Synectin accomplishes this in part by binding to APPL (adaptor protein, phosphotyrosine interaction, PH domain and leucine zipper containing), a protein that recruits RAB5 to enlarged APPL-associated membrane structures, a key event in regulation of signal transduction (Chial et al., 2008; Miaczynska et al., 2004), and in part by binding to myosin-VI.

Myosin-VI, unlike other myosins, is able to move towards the minus end of actin filaments, and as a result it has been implicated in a variety of cellular processes including endocytosis, secretion and membrane ruffling (Buss and Kendrick-Jones, 2008). Furthermore, myosin-VI

colocalizes with synectin in uncoated endocytic vesicles and is involved in their movement through the cortical actin filament network below the plasma cell membrane(Chibalina et al., 2007).

In the present study we extend these observations by demonstrating that the synectin-myosin-VI dependent transport of VEGFR2-containing endosomes plays a key role in the regulation of VEGF signaling and arterial specification. Homozygous disruption of both synectin and myosin-VI expression in mice or knockdown of their expression in zebrafish results in similar phenotypes highlighted by decreased arterial morphogenesis including reduced size of the arterial vasculature, reduced branching and the inability to restore arterial perfusion in adult tissues. These phenotypes can be traced to reduced activation of the Y^{1175} site on VEGFR2 that is specifically involved in activation of the PLCγ-MAPK pathway that has been implicated in arterial morphogenesis. In turn, the proximal cause of reduced Y^{1175} phosphorylation is slow trafficking of VEGFR2 endosomes from the cortical zone where it is exposed to PTP1b that dephosphorylates this site. The impairment of VEGF signaling in this case is not complete as eventually some VEGFR2 endosomes are able to move away from the plasma cell membrane and some degree of PLCγ and ERK-1/2 activation is maintained. As a result, the deletion of either synectin or myosin-VI is not lethal but both are associated with impaired arterial morphogenesis.

The links between these events are demonstrated by the ability of full-length synectin to restore the phenotype in synectin null endothelial cells while mutants with disrupted myosin-VI or PDZ binding sites have no such activity. The latter mutant prevents synectin from binding to APPL and is consistent with a report of suppressed Akt phosphorylation that depends on Y^{1175} phosphorylation (Saito et al., 2007). The link to PTP1b is suggested by restoration of VEGF signaling in synectin null cells following suppression of PTP1b expression while knockdown of other VEGFR2-associated PTPs have less effect. Furthermore, arterial morphogenesis was restored in adult synectin$^{-/-}$ mice following suppression of PTP1b activity using a specific inhibitor in an ischemic setting. Finally, PTP1b knockdown largely restored developmental arterial morphogenesis abnormalities in myosin-VI^{KD} zebrafish.

The findings in this study suggest the following sequence of events. Following VEGF binding, VEGFR2 is activated as demonstrated by phosphorylation of $Y^{1054/1059}$ sites. This in turn leads to auto-phosphorylation of other VEGFR2 tyrosines. The newly activated receptors are then endocytosed, enter the sub-membrane space in clathrin-positive vesicles and bind APPL (Miaczynska et al., 2004) which in turn binds the synectin-myosin-VI complex (Lin et al., 2006; Varsano et al., 2006) that moves VEGFR2 vesicles to EEA1-positive endosomes. At that point, phosphorylation of the Y^{1175} becomes manifest leading to activation of the PLCγ/MAPK and PI3K-Akt cascades. This, in turn, promotes arteriogenic signaling, likely via activation of Ets transcription factors (De Val and Black, 2009; Watanabe et al., 2004).

In the absence of synectin or myosin-VI, the VEGFR2-containing vesicles spend an excessively long time in the sub-membrane region where the Y^{1175} site is dephosphorylated by PTP1b, leading to selective downregulation of PI3K/Akt and MAPK cascades thus resulting in defective arteriogenesis and branching morphogenesis. On the other hand, knockdown of Rab7 or Rab11 expression increases ERK activation as it forces the VEGFR2 endosome to spend more time in the “signaling compartment” of the cytoplasm

In conclusion, our findings identify the synectin/myosin-VI complex as a key regulator of arterial morphogenesis and demonstrate that trafficking of VEGFR2-containing endocytic vesicles results in selective regulation of VEGF receptor 2 signaling.

METHODS

Reagents and Antibodies

The list of antibodies and other reagents is presented in the web supplement (S1)

Isolation of murine arterial and veinous endothelial cells

Primary arterial and venous endothelial cells were isolated from adult mouse dorsal aorta and vena cava using a protocol similar to that previously described (Allport et al., 2002).

Adenovirus Rescue of Endothelial Cells

Cells were plated on 10 cm fibronectin coated dishes, grown to 60–70% confluence and starved for 8 hours in media containing 0.5% FBS. Adenovirus was added overnight in media containing 0.5% FBS at an MOI of 100 and the next day media containing 20% FBS was added. After 2–3 days the cells were starved overnight in 0.5% FBS and stimulated with VEGF-A_{165}(50ng/ml) for 5 minutes then harvested with RIPA lysis buffer.

siRNA Transfection of Endothelial Cells

200pmoles/dish of siRNA(Qiagen) in 1ml media containing 0.5% FBS and Targefect siRNA suspension(Targeting Systems) was added to cells plated on 6cm fibronectin coated dishes at 70–80% confluent and incubated for 2hrs at 37°C. The same procedure was repeated 24 hr later.

Analysis of VEGFR-2 Internalization by Cell-Surface Biotinylation

Cells were grown to confluence on 10cm fibronectin coated dishes and starved overnight in media with 0.5%FBS. After rinsing with cold PBS, cells were incubated with 5ml/dish EZ-Link Sulfo-NHS-SS-Biotin(0.25mg/ml) in PBS at 4°C for 30 min., quenched with cold PBS + 50mM glycine and rinsed with cold media with 1% BSA. Cells were then stimulated with VEGF-A (50ng/ml) at 37°C for. At pre-determined time points cells were rinsed with cold PBS and incubated for 20 min. on ice with glutathione (45mM) in 75mM NaCL, 75mM NaOH, 1mM EDTA, 1% BSA. Glutathione was quenched with cold PBS with iodoacetamide (5mg/ml). Cells were rinsed with cold PBS and protein lysates prepared using NP-40 lysis buffer. 200 μg of lysate was immunoprecipitated with 50 μl of NeutrAvidin beads at 4°C overnight, then rinsed with 500 μl of NP-40 lysis buffer and resuspended in 60 μl 2× Lamelli`s SDS-sample buffer. Samples were analyzed by SDS-PAGE followed by Western blotting with anti-VEGFR2 (Cell Signaling).

Endothelial Cell Migration Assay

Cell migration was measured by “wounding” assays as previously described (Chittenden et al., 2006) Cells were treated with medium containing 0.5% FBS, 20% FBS or 0.5% FBS plus VEGF (50ng/ml). An average of at least 10 measurements per condition from 2 individual wells were analyzed for each experiment.

Colocalization of VEGFR-2 and EEA1, Rab7 and Rab11

Cells were plated on fibronectin coated glass-bottom plates (MatTek) and starved overnight with 0.5%FBS. All antibody labelings were carried out on ice. Cells were labeled with rat anti-mouse VEGFR-2(10μg/ml) primary antibody for 15 min., rinsed with cold PBS, followed by chick anti-rat alexa488 secondary antibody for 15 min. Cells were then stimulated with VEGF-A_{165}(50ng/ml) and following incubation at 37°C for 0–30min., cells were washed with ice cold PBS pH 2.5 to remove remaining cell surface receptors. Cells were fixed for 10 min. at 25°C 4% paraformaldehyde and permeablized with 2.5% PFA/0.1% Triton X-100/0.1% NP-40 for

10 min. Cells were then labeled with goat anti-EEA1 antibody overnight, followed by chick anti-goat alexa647 secondary antibody. Samples were observed under a wide field fluorescence microscope (Olympus IX-71) equipped with a Sensicam QE cooled CCD camera (Cooks), DG-4 xenon arc light source (Sutter) and 60× oil immersion lens. QED software (Media Cybernetics) was used for image acquisitions. Co-localization was quantified using the co-localization plugin of Image J. For co-localization of Rab7(Rab11) cells were labeled with mouse anti-Rab7(Rab11) followed by rabbit anti-mouse alexa568 secondary antibody. Images were acquired by laser-scanning confocal microscopy with X63 objective (Zeiss LSM 510 Meta).

Live Cell Microscopic Imaging of VEGFR-2 Containing Vesicles

Cells were labeled with rat anti-mouse monoclonal VEGFR2 (10μg/ml) primary antibody for 15 min., rinsed with cold PBS, labeled with chick anti-rat alexa488 secondary antibody for 15 min. and rinsed again with cold PBS. Cells were placed on the microscope stage and treated with media supplemented with 0.5%FBS and VEGF-A_{165}(50ng/ml) at 37°C. Time-lapse imaging was done on an inverted microscope (Olympus IX-71 widefield) equipped with a plexiglass-enclosed stage kept at 37°C and 5% CO_2. Images were acquired by a cooled software-controlled (QED, Media Cybernetics) charge-coupled device camera (SensiCam, Cooke Corp) using a filter and a 60× oil immersion objective lens (Olympus). Images were acquired every 30 seconds for 30 min. following VEGF stimulation. Images were processed using ImageJ and individual vesicles were tracked using the “manual tracking” plugin.

Surgical Hindlimb Ischemia Model

This was done as previously described (Chittenden et al., 2006). Laser-Doppler flow imaging was carried out using a Moor Infrared Laser Doppler Imager (LDI; Moor Instruments Ltd) at 36.5°C to 37.5°C under isoflurane anesthesia. The data were analyzed with Moor LDI image processing software V3.09 and reported as the ratio of flow in the right/left (R/L) hindlimb.

Micro-CT Angiography

A 1:1 mixture of bismuth (Sigma-Aldrich) and gelatin (ICN Biomedicals) was used as the vascular contrast agent. The preparation, acquisition and analysis of micro-CT images was carried out as previously described (Chittenden et al., 2006).

PTP1B inhibitor treatment

PTP1B inhibitor was synthesized and provided by Merck Frosst Canada and used as previously described (Julien et al., 2007). PTP1B compound (or vehicle) was administered (30mg/kg body weight) daily by oral gavage with an injection volume of 10ml/kg body weight beginning two days prior to femoral artery ligation. Vehicle solution consisted of 0.5% methylcellulose (Sigma Aldrich).

Zebrafish analysis

Zebrafish morpholino knockdown—*Tg(fli1:EGFP)*^{y1} zebrafish (Lawson and Weinstein, 2002) were maintained under standard laboratory conditions. Embryos were kept in 0.3× Danieau/PTU (embryo water) at 28°C. The following gene-specific and control antisense morpolino oligonucleotides were purchased from Gene Tools (LLC, Corvallis) (see Supplementary Methods for sequence details). Silencing efficiencies of Myo6a-ATG1, Myo6a-ATG2 and Ptp1b-ATG were determined as previously described using a luciferase reporter assay (Ny et al., 2005), whereas silencing efficiency of Ptp1b-Splice was evidenced by PCR amplification of ptp1b-specific sequences, spanning the first intron boundary, using cDNA from ptp1b-Splice-injected embryos of 2 dpf. Different doses of morpholinos and, for the rescue experiments, different combinations of morpholinos, were injected into single- to

four-cell stage embryos, using procedures as previously described (Stalmans et al., 2002) and embryos were further incubated in embryo water at 28°C until 16 hpf, 30 hpf and 40 hpf. At these time points, between 30 and 60 injected embryos per experiment were analyzed. The penetrance per experiment was scored by counting the affected embryos and each experiment was repeated at least three times. All data of myo6a knockdown shown in the manuscript were obtained after injection of 10.5 ng of Myo6a-ATG1. Control embryos were injected with injection buffer (0.1% phenol red, 0.4M KCl). Confocal imaging of embryos was performed using a Zeiss laser scanning microscope LSM510 and the 488 nm laser emission was supplied by an argon laser.

Zebrafish whole-mount in situ hybridization and immunostaining—Dechorionated embryos were fixed overnight in 4% paraformaldehyde at 4°C. Whole-mount *in situ* hybridization was performed as described (Stalmans et al., 2002), using antisense probes for zebrafish *myo6a*. *Tg(fli1:EGFP)*^{y1} embryos were immunostained as described with rabbit anti-GFP antibody (Torrey-Pines Biolabs) and mouse anti-BrdU antibody (Santa Cruz Biotechnology). Stained embryos were first embedded in 1.5 % agarose and subsequently in paraffin and sectioned at 7 mm. Sections were counterstained with nuclear fast red and DAPI for hybridized and immunostained embryos respectively. Analysis was performed using a Zeiss Axia Imager microscope.

Statistical Analysis

Standard deviations are shown as bars in the histograms, except for the Hindlimb data where the error bars represent standard error of the mean(SEM). Differences were considered statistically significant if p 0.05 by Student's two-tailed *t* test. For the zebrafish analysis, Chi-square analysis was used to determine whether the fraction of embryos exhibiting a certain blood vessel phenotype differed between treatment groups.

Supplementary Material

Refer to Web version on PubMed Central for supplementary material.

Acknowledgments

We would like to thank Arie Horowitz (Cleveland Clinic Foundation) for myosin VI constructs, Yan Huang (Yale) for preparing adenoviruses, Brian Kennedy and Robert Gordon at Merck Frosst for providing the PTP1B inhibitor and advice regarding its use.

Supported in part by NIH grant HL84619 (MS) and a Leducq Foundation Transatlantic Network grant (MS, FJG and PC).

REFERECES

Allport JR, Lim YC, Shipley JM, Senior RM, Shapiro SD, Matsuyoshi N, Vestweber D, Luscinskas FW. Neutrophils from MMP-9- or neutrophil elastase-deficient mice show no defect in transendothelial migration under flow in vitro. J Leukoc Biol 2002;71:821–828. [PubMed: 11994507]

Aschenbrenner L, Naccache SN, Hasson T. Uncoated endocytic vesicles require the unconventional myosin, Myo6, for rapid transport through actin barriers. Mol Biol Cell 2004;15:2253–2263. [PubMed: 15004223]

Bourdeau A, Dube N, Tremblay ML. Cytoplasmic protein tyrosine phosphatases, regulation and function: the roles of PTP1B and TC-PTP. Curr Opin Cell Biol 2005;17:203–209. [PubMed: 15780598]

Buss F, Kendrick-Jones J. How are the cellular functions of myosin VI regulated within the cell? Biochem Biophys Res Commun 2008;369:165–175. [PubMed: 18068125]

Cai H, Reed RR. Cloning and characterization of neuropilin-1-interacting protein: a PSD-95/Dlg/ZO-1 domain-containing protein that interacts with the cytoplasmic domain of neuropilin-1. J Neurosci 1999;19:6519–6527. [PubMed: 10414980]

Chabot C, Spring K, Gratton JP, Elchebly M, Royal I. New role for the protein tyrosine phosphatase DEP-1 in Akt activation and endothelial cell survival. Mol Cell Biol 2009;29:241–253. [PubMed: 18936167]

Chial HJ, Wu R, Ustach CV, McPhail LC, Mobley WC, Chen YQ. Membrane targeting by APPL1 and APPL2: dynamic scaffolds that oligomerize and bind phosphoinositides. Traffic 2008;9:215–229. [PubMed: 18034774]

Chibalina MV, Seaman MN, Miller CC, Kendrick-Jones J, Buss F. Myosin VI and its interacting protein LMTK2 regulate tubule formation and transport to the endocytic recycling compartment. J Cell Sci 2007;120:4278–4288. [PubMed: 18029400]

Chittenden TW, Claes F, Lanahan AA, Autiero M, Palac RT, Tkachenko EV, Elfenbein A, Ruiz de Almodovar C, Dedkov E, Tomanek R, et al. Selective regulation of arterial branching morphogenesis by synectin. Dev Cell 2006;10:783–795. [PubMed: 16740480]

Dance AL, Miller M, Seragaki S, Aryal P, White B, Aschenbrenner L, Hasson T. Regulation of myosin-VI targeting to endocytic compartments. Traffic 2004;5:798–813. [PubMed: 15355515]

De Val S, Black BL. Transcriptional control of endothelial cell development. Dev Cell 2009;16:180–195. [PubMed: 19217421]

De Vries L, Lou X, Zhao G, Zheng B, Farquhar MG. GIPC, a PDZ domain containing protein, interacts specifically with the C terminus of RGS-GAIP. Proc Natl Acad Sci U S A 1998;95:12340–12345. [PubMed: 9770488]

Di Fiore PP, De Camilli P. Endocytosis and signaling. an inseparable partnership. Cell 2001;106:1–4. [PubMed: 11461694]

Eden ER, White IJ, Futter CE. Down-regulation of epidermal growth factor receptor signalling within multivesicular bodies. Biochem Soc Trans 2009;37:173–177. [PubMed: 19143625]

Gao Y, Li M, Chen W, Simons M. Synectin, syndecan-4 cytoplasmic domain binding PDZ protein, inhibits cell migration. J Cell Physiol 2000;184:373–379. [PubMed: 10911369]

Haj FG, Verveer PJ, Squire A, Neel BG, Bastiaens PI. Imaging sites of receptor dephosphorylation by PTP1B on the surface of the endoplasmic reticulum. Science 2002;295:1708–1711. [PubMed: 11872838]

Julien SG, Dube N, Read M, Penney J, Paquet M, Han Y, Kennedy BP, Muller WJ, Tremblay ML. Protein tyrosine phosphatase 1B deficiency or inhibition delays ErbB2-induced mammary tumorigenesis and protects from lung metastasis. Nat Genet 2007;39:338–346. [PubMed: 17259984]

Kappler JA, Starr CJ, Chan DK, Kollmar R, Hudspeth AJ. A nonsense mutation in the gene encoding a zebrafish myosin VI isoform causes defects in hair-cell mechanotransduction. Proc Natl Acad Sci U S A 2004;101:13056–13061. [PubMed: 15317943]

Lampugnani MG, Orsenigo F, Gagliani MC, Tacchetti C, Dejana E. Vascular endothelial cadherin controls VEGFR-2 internalization and signaling from intracellular compartments. J Cell Biol 2006;174:593–604. [PubMed: 16893970]

Lampugnani MG, Zanetti A, Corada M, Takahashi T, Balconi G, Breviario F, Orsenigo F, Cattelino A, Kemler R, Daniel TO, et al. Contact inhibition of VEGF-induced proliferation requires vascular endothelial cadherin, beta-catenin, and the phosphatase DEP-1/CD148. J Cell Biol 2003;161:793–804. [PubMed: 12771128]

Lanahan AA, Chittenden TW, Mulvihill E, Smith K, Schwartz S, Simons M. Synectin-dependent gene expression in endothelial cells. Physiol Genomics 2006;27:380–390. [PubMed: 16940428]

Lawson ND, Weinstein BM. In vivo imaging of embryonic vascular development using transgenic zebrafish. Developmental biology 2002;248:307–318. [PubMed: 12167406]

Lin DC, Quevedo C, Brewer NE, Bell A, Testa JR, Grimes ML, Miller FD, Kaplan DR. APPL1 associates with TrkA and GIPC1 and is required for nerve growth factor-mediated signal transduction. Mol Cell Biol 2006;26:8928–8941. [PubMed: 17000777]

Lou X, Yano H, Lee F, Chao MV, Farquhar MG. GIPC and GAIP form a complex with TrkA: a putative link between G protein and receptor tyrosine kinase pathways. Mol Biol Cell 2001;12:615–627. [PubMed: 11251075]

Mattila E, Auvinen K, Salmi M, Ivaska J. The protein tyrosine phosphatase TCPTP controls VEGFR2 signalling. J Cell Sci 2008;121:3570–3580. [PubMed: 18840653]

Mellberg S, Dimberg A, Bahram F, Hayashi M, Rennel E, Ameur A, Westholm JO, Larsson E, Lindahl P, Cross MJ, et al. Transcriptional profiling reveals a critical role for tyrosine phosphatase VE-PTP in regulation of VEGFR2 activity and endothelial cell morphogenesis. Faseb J. 2009

Miaczynska M, Christoforidis S, Giner A, Shevchenko A, Uttenweiler-Joseph S, Habermann B, Wilm M, Parton RG, Zerial M. APPL proteins link Rab5 to nuclear signal transduction via an endosomal compartment. Cell 2004;116:445–456. [PubMed: 15016378]

Milarski KL, Zhu G, Pearl CG, McNamara DJ, Dobrusin EM, MacLean D, Thieme-Sefler A, Zhang ZY, Sawyer T, Decker SJ, et al. Sequence specificity in recognition of the epidermal growth factor receptor by protein tyrosine phosphatase 1B. J Biol Chem 1993;268:23634–23639. [PubMed: 7693694]

Mitola S, Brenchio B, Piccinini M, Tertoolen L, Zammataro L, Breier G, Rinaudo MT, den Hertog J, Arese M, Bussolino F. Type I collagen limits VEGFR-2 signaling by a SHP2 protein-tyrosine phosphatase-dependent mechanism 1. Circ Res 2006;98:45–54. [PubMed: 16339483]

Naccache SN, Hasson T, Horowitz A. Binding of internalized receptors to the PDZ domain of GIPC/synectin recruits myosin VI to endocytic vesicles. Proc Natl Acad Sci U S A 2006;103:12735–12740. [PubMed: 16908842]

Nakamura Y, Patrushev N, Inomata H, Mehta D, Urao N, Kim HW, Razvi M, Kini V, Mahadev K, Goldstein BJ, et al. Role of protein tyrosine phosphatase 1B in vascular endothelial growth factor signaling and cell-cell adhesions in endothelial cells. Circ Res 2008;102:1182–1191. [PubMed: 18451337]

Nottebaum AF, Cagna G, Winderlich M, Gamp AC, Linnepe R, Polaschegg C, Filippova K, Lyck R, Engelhardt B, Kamenyeva O, et al. VE-PTP maintains the endothelial barrier via plakoglobin and becomes dissociated from VE-cadherin by leukocytes and by VEGF. J Exp Med 2008;205:2929–2945. [PubMed: 19015309]

Ny A, Koch M, Schneider M, Neven E, Tong RT, Maity S, Fischer C, Plaisance S, Lambrechts D, Heligon C, et al. A genetic Xenopus laevis tadpole model to study lymphangiogenesis. Nature medicine 2005;11:998–1004.

Prahst C, Heroult M, Lanahan AA, Uziel N, Kessler O, Shraga-Heled N, Simons M, Neufeld G, Augustin HG. Neuropilin-1-VEGFR-2 complexing requires the PDZ-binding domain of neuropilin-1. J Biol Chem 2008;283:25110–25114. [PubMed: 18628209]

Saito T, Jones CC, Huang S, Czech MP, Pilch PF. The interaction of Akt with APPL1 is required for insulin-stimulated Glut4 translocation. J Biol Chem 2007;282:32280–32287. [PubMed: 17848569]

Sakurai Y, Ohgimoto K, Kataoka Y, Yoshida N, Shibuya M. Essential role of Flk-1 (VEGF receptor 2) tyrosine residue 1173 in vasculogenesis in mice. Proc Natl Acad Sci U S A 2005;102:1076–1081. [PubMed: 15644447]

Seiler C, Ben-David O, Sidi S, Hendrich O, Rusch A, Burnside B, Avraham KB, Nicolson T. Myosin VI is required for structural integrity of the apical surface of sensory hair cells in zebrafish. Developmental biology 2004;272:328–338. [PubMed: 15282151]

Stalmans I, Ng YS, Rohan R, Fruttiger M, Bouche A, Yuce A, Fujisawa H, Hermans B, Shani M, Jansen S, et al. Arteriolar and venular patterning in retinas of mice selectively expressing VEGF isoforms. The Journal of clinical investigation 2002;109:327–336. [PubMed: 11827992]

Tkachenko E, Elfenbein A, Tirziu D, Simons M. Syndecan-4 clustering induces cell migration in a PDZ-dependent manner. Circ Res 2006;98:1398–1404. [PubMed: 16675718]

Valdembri D, Caswell PT, Anderson KI, Schwarz JP, Konig I, Astanina E, Caccavari F, Norman JC, Humphries MJ, Bussolino F, et al. Neuropilin-1/GIPC1 signaling regulates alpha5beta1 integrin traffic and function in endothelial cells. PLoS Biol 2009;7:e25. [PubMed: 19175293]

van der Sar AM, de Fockert J, Betist M, Zivkovic D, den Hertog J. Pleiotropic effects of zebrafish protein-tyrosine phosphatase-1B on early embryonic development. Int J Dev Biol 1999;43:785–794. [PubMed: 10707902]

Varsano T, Dong MQ, Niesman I, Gacula H, Lou X, Ma T, Testa JR, Yates JR 3rd, Farquhar MG. GIPC is recruited by APPL to peripheral TrkA endosomes and regulates TrkA trafficking and signaling. Mol Cell Biol 2006;26:8942–8952. [PubMed: 17015470]

von Zastrow M, Sorkin A. Signaling on the endocytic pathway. Curr Opin Cell Biol 2007;19:436–445. [PubMed: 17662591]

Wang LH, Kalb RG, Strittmatter SM. A PDZ protein regulates the distribution of the transmembrane semaphorin, M-SemF. J Biol Chem 1999;274:14137–14146. [PubMed: 10318831]

Watanabe D, Takagi H, Suzuma K, Suzuma I, Oh H, Ohashi H, Kemmochi S, Uemura A, Ojima T, Suganami E, et al. Transcription factor Ets-1 mediates ischemia- and vascular endothelial growth factor-dependent retinal neovascularization. Am J Pathol 2004;164:1827–1835. [PubMed: 15111329]

Wieman HL, Horn SR, Jacobs SR, Altman BJ, Kornbluth S, Rathmell JC. An essential role for the Glut1 PDZ-binding motif in growth factor regulation of Glut1 degradation and trafficking. Biochem J 2009;418:345–367. [PubMed: 19016655]

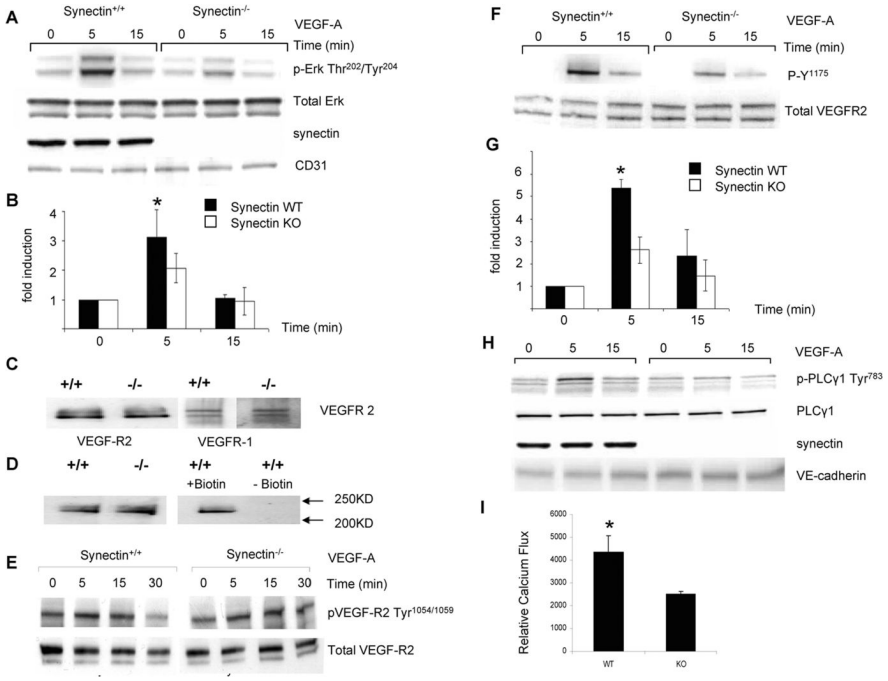

Figure 1. VEGF-A Signaling in Synectin$^{-/-}$ Primary Endothelial Cells

(A,B) *ERK activation* A: Western blotting of total cell lysates isolated from synectin$^{+/+}$ and $^{-/-}$ endothelial cells. Confluent, serum starved cells were stimulated for the times indicated with 50ng/ml VEGF-A. Phosphorylation of p44/42 MAP kinase in response to VEGF-A is reduced in synectin$^{-/-}$ cells relative to synectin$^{+/+}$ cells. B: Quantification of ERK activation in 4 independent experiments (Mean±SD, * $P < 0.05$)

(C,D) *VEGF receptor expression*. Expression of VEGFR1 and VEGFR2 in synectin$^{+/+}$ and $^{-/-}$ AEC. C: Western blotting of total cell lysates following cell surface biotinylation and precipitation of 200ug of protein lysate with NeutrAvidin beads. Note comparable cell surface levels of VEGFR-1 and 2 in synectin$^{+/+}$ and $^{-/-}$ endothelial cells. D: Western blotting of biotinylated cell extracts with VEGFR2 antibody following precipitation of 200ug of protein lysate with NeutrAvidin beads. The right panel represents a control for nonspecific precipitation of VEGFR-2 and shows that, in the absence of biotinylation, VEGFR2 is not precipitated.

(E, F,G) *VEGFR2 activation*: VEGF-A activation of VEGFR2 Y^{1175} but not $Y^{1054/1059}$ is decreased in synectin$^{-/-}$ AEC: Western blotting of total cell lysates from synectin$^{+/+}$ and $^{-/-}$ AEC following serum starvation and stimulation with 50ng/ml VEGF-A. Note reduced phosphorylation of the Y1175 site in synectin$^{-/-}$ AEC. G: Quantitative analysis of VEGFR2 Y^{1175} site phosphorylation based on 4 independent experiments. (Mean±SD, * $P < 0.05$) (H) *PLCγ activation*: VEGF-A activation of PLCγ in synectin$^{-/-}$ AEC: Western blotting of total cell lysates isolated from synectin$^{+/+}$ and $^{-/-}$ AEC following serum starvation and stimulation with 50ng/ml VEGF-A. Note reduced phosphorylation of the Y1175 site in synectin$^{-/-}$ AEC. G: Quantitative analysis of VEGFR2 Y^{1175} site phosphorylation based on 4 independent experiments. (Mean±SD, * $P < 0.05$)

(H) *PLCγ activation*: VEGF-A activation of PLCγ in synectin$^{-/-}$ AEC: Western blotting of total cell lysates isolated from synectin$^{+/+}$ and $^{-/-}$ AEC following serum starvation and stimulation with 50ng/ml VEGF-A. Note reduced phosphorylation of PLCγ1 on tyrosine 783 in synectin$^{-/-}$ AEC. See also Fig S1.

(I) *Calcium flux*: VEGF-A induced calcium levels in synectin$^{-/-}$ AEC: Calcium flux in synectin$^{+/+}$ and $^{-/-}$ AEC was measured after overnight starvation, in cells loaded with 5uM

Indo-1-AM following VEGF-A(250ng/ml) stimulation. Note reduced calcium flux in synectin$^{-/-}$ AEC. (Mean±SD, * $P < 0.05$). See also Supplementary materials.

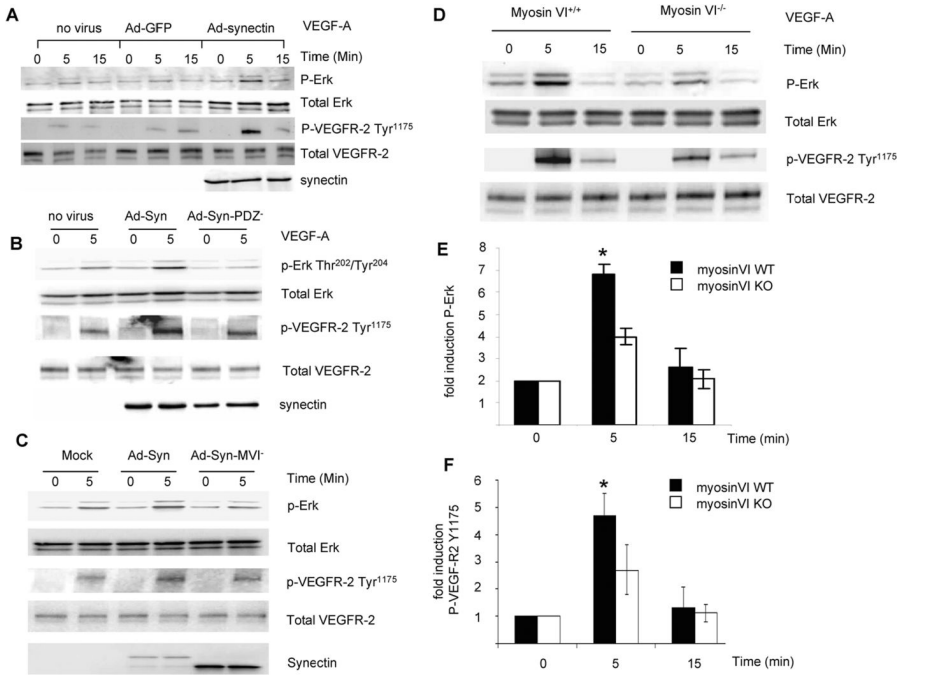

Figure 2. Role of synectin-interacting proteins in VEGF signaling

(A–C) *Synectin rescue of VEGF signaling in synectin$^{-/-}$ AEC*: Synectin$^{-/-}$ AEC were transduced with adenovirus containing either GFP, full length synectin (Ad-Syn, Panel A), synectin with a mutant PDZ domain (Ad-Syn-PDZ^{-}, Panel B) or synectin with a mutant myosin-VI binding site (Ad-Syn-MVI-, Panel C) for 2 days, starved, and stimulated with 50ng/ml VEGF-A. Western blotting of total cell lysates with pErk(Thr^{202}/Tyr^{204}) and pVEGFR-2 (Tyr^{1175}) shows that expression of Ad-Syn but not Ad-Syn-PDZ^{-} or Ad-Syn-MVI^{-} restores VEGF activation of VEGFR2 and ERK in synectin$^{-/-}$ AEC.

(D–F) VEGF-A activation of p44/42 MAP kinase and VEGFR2 is reduced in myosin-VI$^{-/-}$ *AEC:* Western blotting of total cell lysates isolated from myosin-VI$^{+/+}$ and $^{-/-}$ AEC. Confluent, serum starved cells were stimulated with 50ng/ml VEGF-A and phosphorylation of ERK1/2 and VEGF-R2 Y^{1175} was then determined. Note reduced activation of both proteins. Quantification of ERK activation (E) and VEGFR2 Y^{1175} (F) was carried out on the basis of 4 independent experiments. (Mean±SD, * $P < 0.05$)

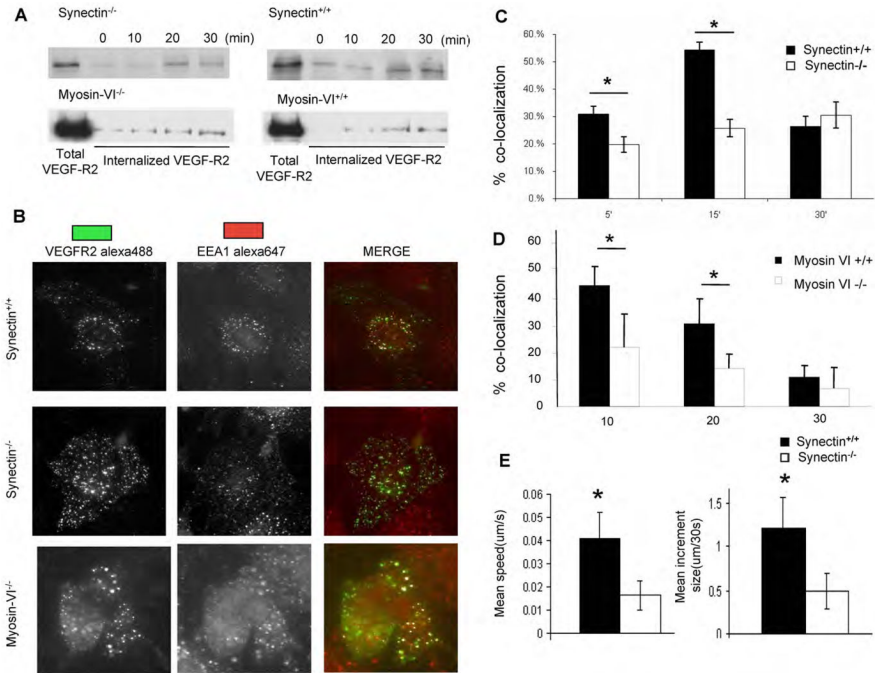

Figure 3. VEGFR-2 Trafficking in Synectin$^{-/-}$ and MyosinVI$^{-/-}$ Primary Endothelial Cells

(A) VEGFR-2 internalization is similar in synectin and myosin-VI$^{+/+}$ *and* $^{-/-}$ *endothelial cells*: Confluent, serum starved cells were surface labeled with biotin and stimulated with VEGF-A. After stripping remaining cell surface biotin, cell lysates were precipitated with NeutrAvidin beads and Western blots probed for VEGFR2 to determine internalized VEGFR2. See also Fig S2.

(B–D) *VEGFR2 trafficking*: Serum starved synectin$^{+/+}$ and $^{-/-}$ or myosin-VI-$^{+/+}$ and $^{-/-}$ AEC cells labeled with anti-VEGFR2(green) were treated with VEGF-A for 5–30min. and then fixed, permeablized, labeled with anti-EEA1(red) and visualized using immunofluorescent microscopy. Quantification of VEGFR2/EEA1 co-localization at various time points is shown for synectin$^{+/+}$ and $^{-/-}$ AEC in panel C and myosin-VI$^{+/+}$ and $^{-/-}$ AEC in panel D. (Mean±SD, * $P < 0.05$)

(E) Movement of VEGFR-2 containing vesicles in synectin$^{-/-}$ *AEC:* Serum starved cells labeled with anti-VEGFR-2 were treated with VEGF-A and the labeled vesicles tracked by time-lapse microscopy. Images were acquired every 30 seconds for 30 minutes and vesicle mean speed and increment were determined using Image J. (Mean±SD, * $P < 0.05$). Sere also Fig S3

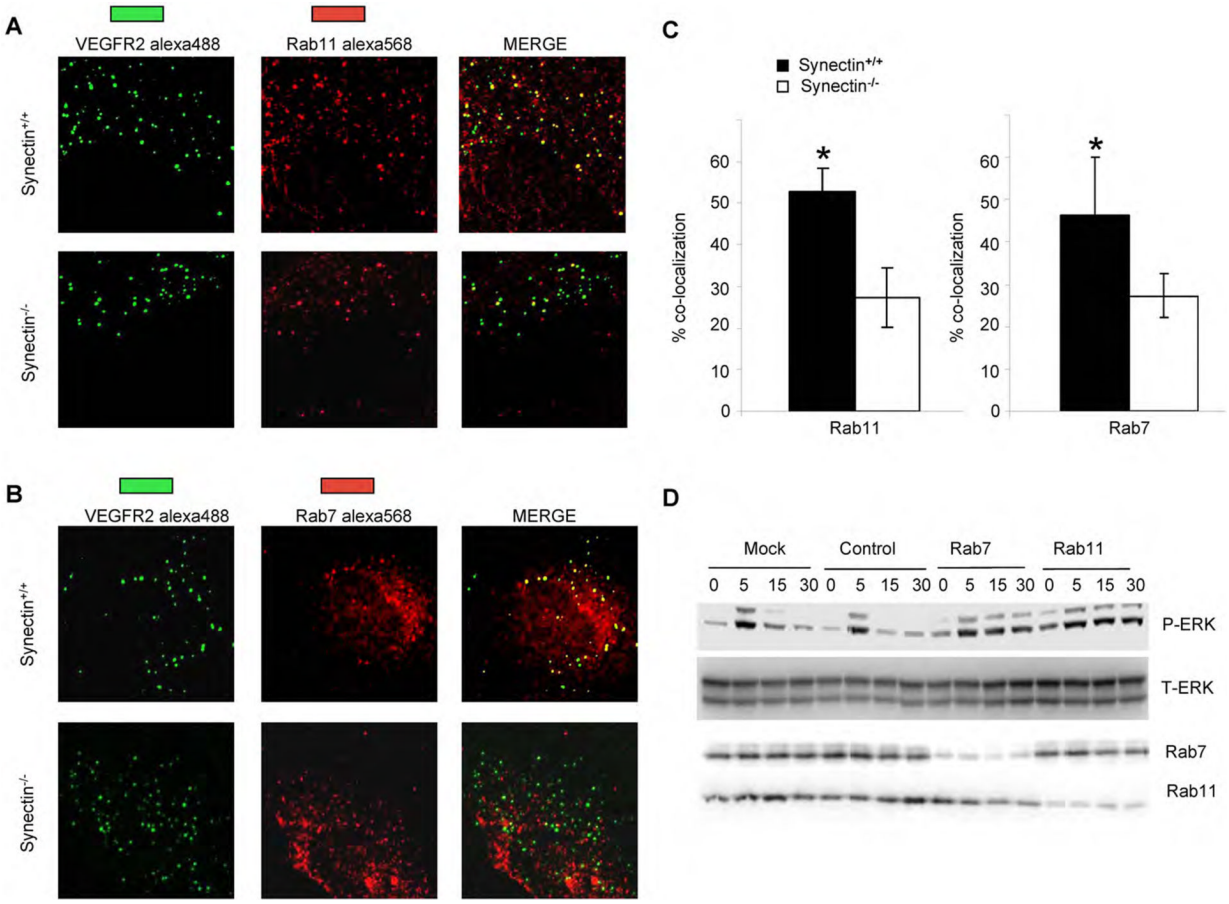

Figure 4. Role of Rab7/Rab11 GTPases in VEGFR2 signaling

(A,B) *Co-localization of VEGFR-2 with endosome markers:* serum starved synectin$^{+/+}$ and $^{-/-}$ AEC were labeled with anti-VEGFR-2(green) and then treated with VEGF-A for 30 minutes, fixed, permeablized and labeled with anti-Rab11(red, panel A) or anti-Rab7 (red, panel B) and processed for confocal microscopy.

(C) Co-localization of VEGFR-2 with Rab11 and Rab7 is delayed in synectin null cells: Quantitative analysis of VEGFR2 colocalization with Rab7 and Rab11 was carried out using the colocalization plugin of Image J in at least 10 independent fields. (Mean±SD, * $P < 0.05$)

(D) Knockdown of Rab7, Rab11 with siRNA Results in Prolonged VEGF-A Activation of p44/42 MAP Kinase: Synectin$^{+/+}$ endothelial cells were transfected with anti-Rab7 or Rab11 siRNAs and 48 hr later, starved overnight and stimulated with 50ng/ml VEGF-A. Western blotting of total cell lysates with pERK shows increased activation following Rab7 and Rab 11 knockdowns.

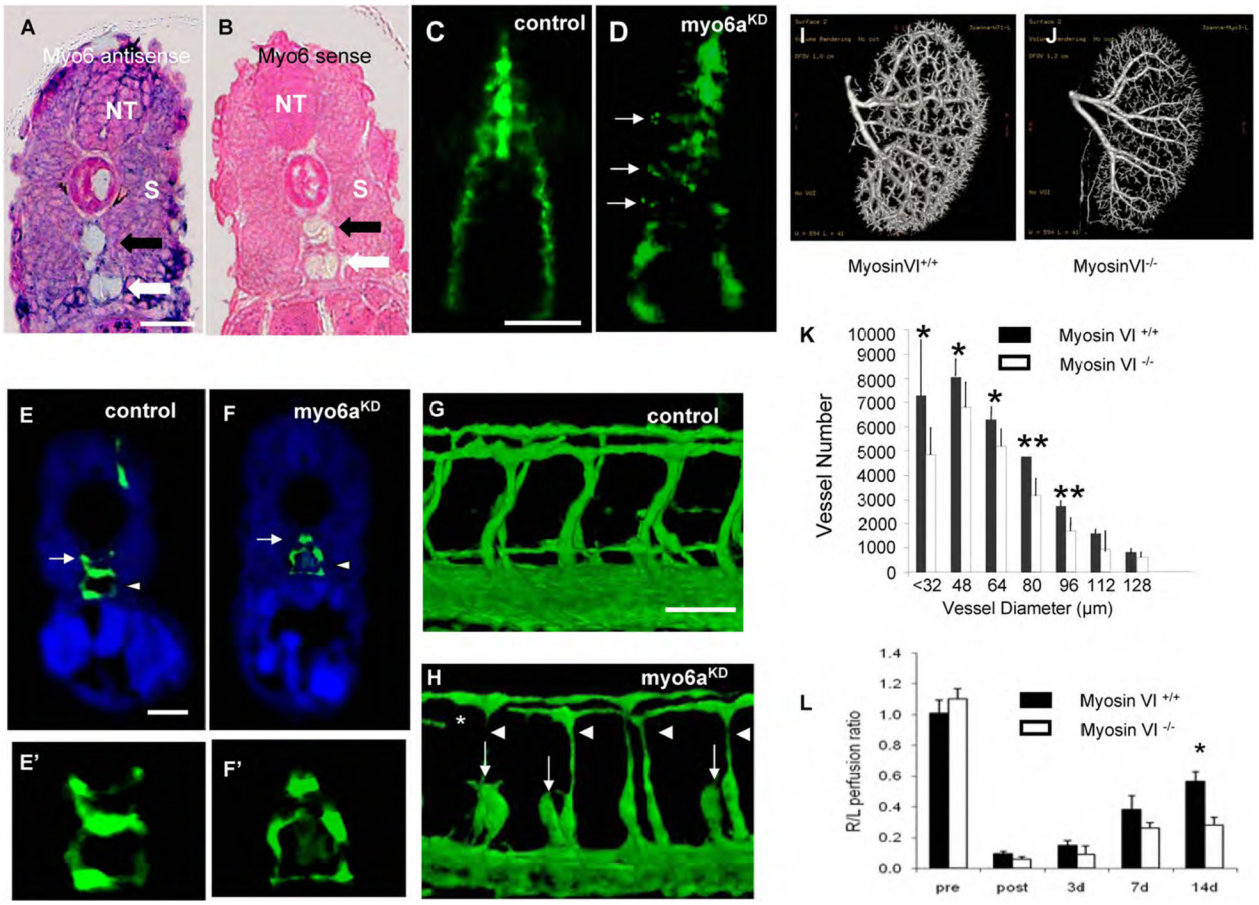

Figure 5. Myo6aKD Impairs Arterial Development in Zebrafish; Functional Effects of Mysosin VI Gene Disruption in Mice

(A,B) Transverse section through the trunk of a 28 hpf zebrafish embryo stained by whole-mount *in situ* hybridization using a myo6a specific antisense (A) or sense (B) riboprobe. Myo6a expression was observed in the neural tube (NT), somites (S) and both the dorsal aorta (black arrow) and posterior cardinal vein (white arrow). The observed expression pattern is specific as no signal was observed upon hybridization using the sense probe. (C,D) Dorsal view of 16 hpf *Tg(fli1:EGFP)*^{y1} embryo, head on top. In control embryos (C) GFP+ angioblasts migrated in an ordered anteroposteriorly directed zipper-like pattern from the lateral plate mesoderm towards the midline where they assembled into the primitive axial vessels. In contrast, in myo6a^{KD} embryos (D) a portion of angioblasts (arrows) stalled along their lateromedial movement and others failed to maintain their correct stereotyped trajectory, resulting in apparently chaotic migration pattern. (E,F) Transverse sections through the trunk of *Tg (fli1:EGFP)*^{y1} embryos of 30 hpf, following a whole-mount immunostaining using an anti-GFP antibody (green) and counterstained with DAPI (blue); head on top. Compared to control embryos (E,E'), myo6a^{KD} embryos had a strikingly thinner dorsal aorta (arrow) with an obvious reduced lumen size, while the posterior cardinal vein (arrowhead) remained unaffected (F,F'). E' and F' are magnifications of the axial vessels in panel E and F, respectively. (G,H) Lateral view on a trunk segment of *Tg(fli1:EGFP)*^{y1} embryos at 40 hpf; head to the left. In control embryos (G) ISVs sprouted bilaterally from the dorsal aorta adjacent to the ventral somite boundaries and navigated upwards to the laterodorsal roof of the neural tube, where they split, elongated and fused to form the DLAV. However, in myo6a^{KD} embryos (H) ISVs often consisted of slender endothelial cells (arrowheads) and/or stalled along their dorsal trajectory

(arrows), thereby impairing proper DLAV formation (asteriks). Scale bars represent 10 μm in panel A,B,E–F' and 5 μm in panel C,D,G,H. See also Fig S3 and S4.

(I,J) Representative reconstructed micro-CT images of whole kidneys (16μm resolution; n=3) from age- and gender-matched (I) myosinVI$^{+/+}$ and (J) myosinVI$^{-/-}$ mice. Note marked reduction in branching in myosinVI$^{-/-}$ mice.

(K) Quantitative analysis of micro-CT images indicates a marked decrease in total number of <100μm diameter vessels in myosinVI$^{-/-}$ mice (white bars) relative to myosinVI$^{+/+}$ mice (black bars). (Mean±SEM, * $P < 0.05$)

(L) Quantitative analysis of laser Doppler images indicates significant alterations in hindlimb reperfusion 14 days after femoral artery ligation in myosinVI$^{-/-}$ mice (white bars) relative to myosinVI$^{+/+}$ mice (black bars). (Mean±SEM, * $P < 0.05$)

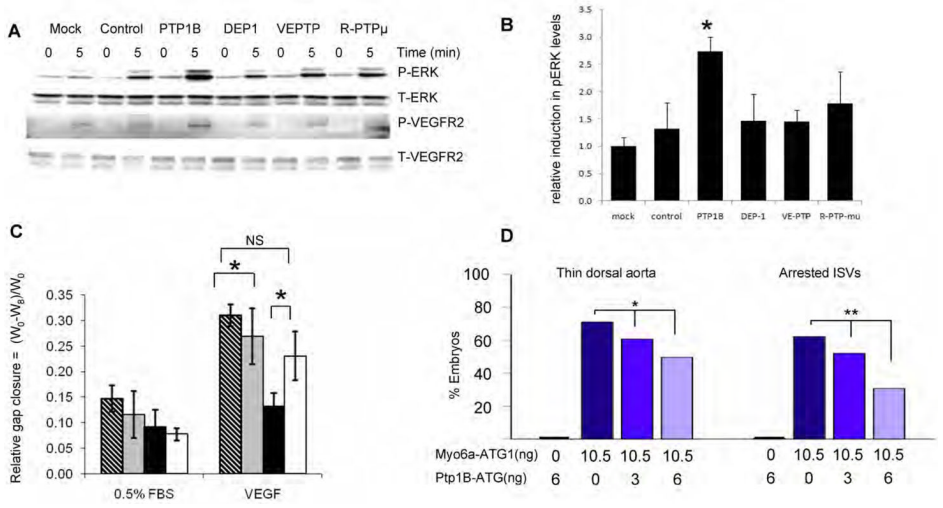

Figure 6. Effect of Phosphatase Knockdown on VEGF signaling

(A,B) PTP1B knockdown increases VEGF signaling in synectin$^{-/-}$ *AEC*. Synectin$^{-/-}$ AEC were transfected with the siRNAs indicated for 2 days, starved, and stimulated with 50ng/ml VEGF-A. Western blotting of total cell lysates with pErk and pVEGFR2(Y^{1175}) shows increased phosphorylation after PTP1b knockdown (Panel A), Quantification of pERK activation is shown in Panel B. (Mean±SEM, * P < 0.05). See also Fig S6.

(C) *Effect of PTP1B knockdown on AEC migration*: The relative distance migrated by AEC from synectin$^{+/+}$ and $^{-/-}$ mice grown on fibronectin coated dishes was measured 8 hrs following `wounding' of a confluent monolayer and stimulation with 0.5%FBS or 50 ng/ml VEGF-A in the presence of either control siRNA or PTP1b siRNA. Note increased extent of migration of synectin$^{-/-}$ cells in response to VEGF following treatment with PTP1B siRNA. Means +/− SD, * = P<0.05. Stippled bars: synectin$^{+/+}$ AEC treated with control siRNA; grey bars: synectin$^{+/+}$ AEC with PTP1b siRNA; black bars: synectin$^{-/-}$ AEC with control siRNA; white bars: synectin$^{-/-}$ AEC with PTP1b siRNA.

(D) Effect of Co-Knockdown of Myo6a and Ptp1b in Zebrafish: Quantitative analysis of arterial defects in morphant embryos revealed that Ptp1b-ATG partially rescues the myo6a knockdown phenotype in a dose-dependent manner. Single ptp1b^{KD} (6ng Ptp1b-ATG) does not induce vascular defects. Dark blue bars indicate single myo6a^{KD} (10.5ng Myo6a-ATG1), blue and light blue bars indicate double ptp1b^{KD}:myo6a^{KD} (10.5ng Myo6a-ATG1 combined with 3 or 6ng Ptp1b-ATG, respectively). *, P<0.05; **, P<0.001.

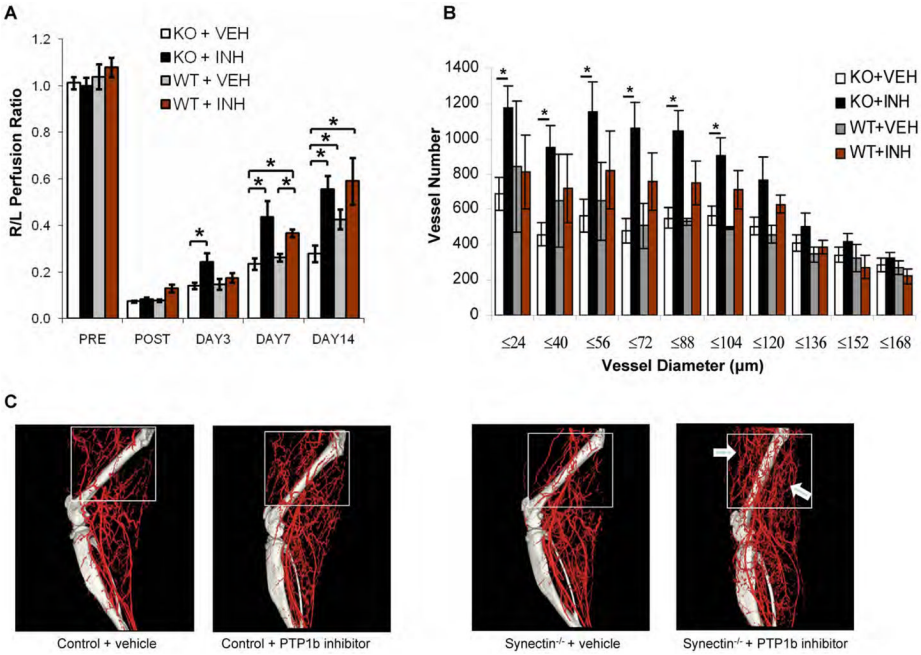

Figure 7. Functional Effects of PTP1B inhibition in synectin$^{-/-}$> mice

(A) *Laser Doppler analysis of blood flow*: synectin$^{-/-}$ and $^{+/+}$ mice were subjected to common femoral artery ligation and PTP1b inhibitor or vehicle were administered as described. The graph shows blood flow in the ischemic foot expressed as a ratio to flow in the normal foot. Note a significant increase in flow in PTP1b inhibitor treated synectin$^{-/-}$ mice. (Mean±SEM, * $P < 0.05$, n=7 per group).

(B,C) Micro CT analysis of arterial vasculature development: Graph (Panel B) shows quantitative analysis of arterial vasculature above the knee in synectin$^{-/-}$ and $^{+/+}$ mice 14 days after common femoral artery ligation and treatment with either PTP1b inhibitor or vehicle. (Mean±SEM, * $P < 0.05$) Note significant increase in smaller size arteries in PTP1b inhibitor treated synectin$^{-/-}$ mice. Representative micro-CT images are shown in Panel C.